mathematics

MDPI

Article

The Casson Dusty Nanofluid: Significance of Darcy–Forchheimer Law, Magnetic Field, and Non-Fourier Heat Flux Model Subject to Stretch Surface

Saif Ur Rehman [1,†], Nageen Fatima [1], Bagh Ali [2], Muhammad Imran [3], Liaqat Ali [4], Nehad Ali Shah [5,*,†] and Jae Dong Chung [5]

1 Department of Mathematics, University of Management and Technology, Lahore 54770, Pakistan
2 Faculty of Computer Science and Information Technology, Superior University, Lahore 54000, Pakistan
3 Department of Mathematics, Government College University, Faisalabad 38000, Pakistan
4 School of Sciences, Xi'an Technological University, Xi'an 710021, China
5 Department of Mechanical Engineering, Sejong University, Seoul 05006, Korea
* Correspondence: nehadali199@sejong.ac.kr
† These authors contributed equally to this work and are co-first authors.

Abstract: This work aims to offer a mathematical model for two-phase flow that investigates the interaction of Casson nanofluid and dust particles across a stretching surface. MHD Darcy–Forchheimer porous medium and Fourier's law through Cattaneo–Christove thermal flux are also considered. The governing equations for the two phases model are partial differential equations later transmuted into ordinary ones via similarity transforms. The Runge–Kutta method with the shooting tool is utilized numerically to solve the boundary layer equations computed in MATLAB to obtain numerical results for various pertinent parameters. The numerical outcomes of momentum, temperature, and concentration distribution are visible for both phases. The results of the skin friction, heat transfer coefficients, and the Sherwood number are also visible in the graphs. Furthermore, by comparing the current findings to the existing literature, the validity of the results is confirmed and found to be in good agreement. The fluid velocity is reduced against increasing strength of Casson fluid parameter, enhanced the fluid phase and dust phase fluid temperature. The temperature declines against the growing values of the relaxation time parameter in both phases. Dusty fluids are used in various engineering and manufacturing sectors, including petroleum transportation, car smoke emissions, power plant pipes, and caustic granules in mining.

Keywords: dust particles; Casson fluid; nanofluid; MHD; Darcy–Forchheimer porous medium; Cattaneo–Christove heat flux

MSC: 00-01; 99-00

check for updates

Citation: Rehman, S.U .; Fatima, N.; Ali, B.; Imran, M.; Ali, L.; Shah, N.A.; Chung, J.D. The Casson Dusty Nanofluid: Significance of Darcy–Forchheimer Law, Magnetic Field, and Non-Fourier Heat Flux Model Subject to Stretch Surface. *Mathematics* **2022**, *10*, 2877. https://doi.org/10.3390/math10162877

Academic Editor: Carlos Llopis-Albert

Received: 24 July 2022
Accepted: 10 August 2022
Published: 11 August 2022

1. Introduction

Due to their two-phase structure, dusty fluid model flows have special researchers' interest in recent studies. This effect occurs in fluid (gas or liquid) flows with the dispersion of solid particles. For illustration, the chemical reaction by which droplets are produced with the coalescence of relatively dust particles and the velocity of dusty air in fluidization difficulties. The fundamental antecedent for planetary systems is created by combining gas and dust particles called cosmic dust. Comet 238 produces tails due to dust particles, and ionized gas being ejected from the comet's core. Many investigators used the dusty phase model to experiment with different flow configurations and boundary constrictions, managing to keep their intrigue in two-phase flows alive. As a result, the solutions they provide are approximate and numerical approaches. Saffman [1] is the one who started the research on dusty fluid laminar flow. The movement of dusty gas in the boundary layer sector was studied by Chakrabarti [2]. Datta and Mishra [3] explored the movement of a dusty liquid across a semi-infinite surface. Wei et al. [4] analyzed the significance of dust particles across a stretching surface.

Newton's viscosity law states that the viscosity should stay constant regardless of stress in a non-Newtonian fluid. Viscosity changes when force is applied to non-Newtonian fluids; either it becomes less viscous or more. Many salt solutions and molten polymers, shampoo, melted butter, blood, toothpaste, and paints are non-Newtonian liquids. Many researchers work on several kinds of non-Newtonian fluids. Anwar et al. [5] deliberated the induced magnetohydrodynamic stream of the non-Newtonian nano-liquid past across a nonlinear stretchable sheet under the impact of thermic conductivity. Kumar et al. [6] analyzed the flow characteristics of non-Newtonian fluid passing across a rotating elliptical cylinder. Khashi et al. [7] analyzed viscous dissipation influence and Magnetohydrodynamic on radiating heat transportation of the non-Newtonian fluid flowing through a nonlinear extending sheet. Chaudhuri et al. [8] deliberated the behavior of MHD in a third-grade non-Newtonian liquid moving over vertical oriented similar plates. Khan et al. [9] presented the bioconvective stream of non-Newtonian nanoparticles with a partial slip under the impacts of unsteady viscosity and Arrhenius activation energy. Across thin peristaltic walls, Riaz et al. [10] studied solid particles' influences on the fluid phase stream of non-newtonian fluid. By imposing slip conditions on the sheet's surface, Ijaz et al. [11]presented a numerical study of the effect of non-linear mixed convection of non-newtonian liquid with entropy generation with thermophoretic effect and joule heating, mass and heat transference in various non-Newtonian fluids towards a stretched surface analyzed by Reddy et al. [12]. Fatunmbi et al. [13] analyzed the nonlinear mixed convection transport of hydromagnetic Casson nanofluid over a nonlinear stretching sheet. Fatunmbi et al. [14] deliberated the boundary layer flow and heat transfer analysis in an electromagnetohydrodynamic dissipative micropolar-Casson fluid over a two-dimensional stretching sheet in the porous medium.

Magnetohydrodynamic (MHD) (hydromagnetics or magnetofluid dynamics) is the study of electrical conducting fluid's behavior and magnetic properties. Liquid metals, plasmas, electrolytes, or saltwater are examples of such magneto liquids. In 1970, Hannes Alfven was awarded the Nobel Prize in Physics for their groundbreaking investigation of MHD. Magnetohydrodynamics has many uses in physics and astronomy, space plasma physics, solar physics, blood pump machines, cancer tumor therapy, and laboratory plasma studies. Sandhya et al. [15] studied the MHD flow under the impacts of mass and heat transference over an inclined plane in the existence of chemical reactions. Kumar et al. [16] studied the time-dependent Eyring–Powell MHD nanofluid past across an angled elastic surface by the Joule heating. Hussain et al. [17] analyzed the thermal transference of nanofluid and MHD stream across a vertical permeable surface. Rehman et al. [18] computed the impacts of radiation on micropolar MHD nanofluid stream over a shrinking surface. MHD nanofluid stream moving across a nonlinear elastic surface associated with convective conditions, examined by Hayat et al. [19]. Kardri et al. [20] discussed the MHD nanofluid stream across a nonlinear shrinking or stretchable cylinder. The general solution of hydromagnetic free convection flow over a moving infinite vertical plate with Newtonian heating, mass diffusion and chemical reaction in the presence of a heat source is completely solved by Fetecau et al. [21].

Khan et al. [22] studied the rotational flow of hybrid MHD nanofluid with entropy generation existence. Shoaib et al. [23] deliberated the numerical solutions of hybrid MHD nanofluid for rotatory motion along with thermic radiation past over an elastic sheet. Hussain et al. [24] analyzed the transfer of heat and 3D time-dependent hydromagnetic flow with the suspension of both nanoparticles and microorganisms. Krishna et al. [25] analyzed the convection behavior of the time-dependent MHD rotating flow under the impacts of thermic radiation past over a moving filled surface numerically. Utilizing the fractional Burgers model and by considering the heat and mass transference, the impacts of MHD, radiation, and chemical reaction are discussed by Jiang et al. [26]. Hossain et al. [27]

analyzed to influence on MHD mixed convective carbon nanotubes nano-fluid utilizing FEM technique numerically. Ghasemi et al. [28] deliberated the impacts of solar radiation on 2D MHD flow of nano-liquid across an extending sheet using the DQM technique. Mandal et al. [29] signified the nanofluid flow in a porous media in the presence of the magnetic field.

A fluid that consists of nanometer-sized small particles forms a colloidal solution of nanoparticles due to suspension in a base fluid. Carbides, metals oxides, and carbon nanotubes are frequently utilized as nanoparticles in nanofluids, with ethylene glycol, oil, and water as base fluids. Choi et al. [30] originated the concept of "Nanofluids" as the small amount of suspension of nanoparticles overdraws the thermal conductivity in a much more reasonable way. Khan et al. [31] analyzed the resistive force impact on Williamson nanofluid flowing across a nonlinear elastic sheet. Saeed et al. [32] studied the convective flow over an angled elastic surface of the thin film nanofluid. Yahya et al. [33] investigated the thermic properties for the hybrid Williamson nanofluid flowing across a stretching sheet with engine oil. Gopal et al. [34] discussed the magnetic and electric strength as well as viscous dissipation for chemical reactions on MHD nanofluid towards a porous extending sheet. Gouran et al. [35] analyzed thermal radiation on magnetohydrodynamics nanofluid stream utilizing two effective computational algorithms. By utilizing the ISPH method, Rashidi et al. [36] studied an updated comprehensive study of the thermophysical properties of hybrid nanofluids and the proposed models. Aly et al. [37] deliberated the impact of magnetic field on nanofluid in the presence of solid particles. Wang et al. [38] analyzed the heat and mass transfer of MHD bio nanofluid across a permeable medium. Sheikholeslami et al. [39] deliberated the recent progress on flat plate solar collectors and photovoltaic systems in the presence of nanofluid.

By studying the all above literature survey, however, we concluded that the research work on the significance of magnetic field, Darcy–Forchheimer law, Bronian motion, and non-Fourier heat flux model on the dynamics of Casson dusty fluid has not been done yet. Motivated by the aforementioned wide scope of non-Newtonian fluid and nanofluid applications, therefore, we decided to evaluate the current elaborated fluid problem. Recently, study on non-Newtonian fluids has fascinated young researchers to extend due to large scale applications in different industries. By using similarity modifications, the relevant nonlinear PDEs are converted into a system of ODEs. The graphical outcomes of velocity, temperature, concentration of nanoparticles, skin friction factor, and Nusselt number are conducted for different inputs of physical parameters. This numerical investigation has many industrials and engineering applications such as including petroleum transportation, power plants, and heat exchangers, etc.

2. Mathematical Formulation

Let us a steady MHD Darcy–Forchhiemer porous medium flow of dusty Casson fluid across a stretching surface. The flow is expected to be restricted to the $y > 0$, and it is created by two equivalent and inverse forces acting along the x-axis and the y-axis, typical to the flow. The sheet is extended along the x-axis at u_x velocity, while a magnetic field of strength B_0 is applied along y-axis as shown in Figure 1. The volume fraction of dust particles is ignored, and the number density is assumed to remain constant. The only way that the fluid and dust particles' motions are linked is by drag and thermal transfer. Stoke's linear drag theory is used to model the drag force. Other communication forces, for example, the virtual force, twist lift force, and shear lift force will be overlooked contrasted with the drag force. Dust particles have a spherical physique, a consistent size, and a constant density. The mathematical model for the flow of the dusty phase, coupled with the constraints, is as follows, based on these physical assumptions and boundary layer approximations [40,41].

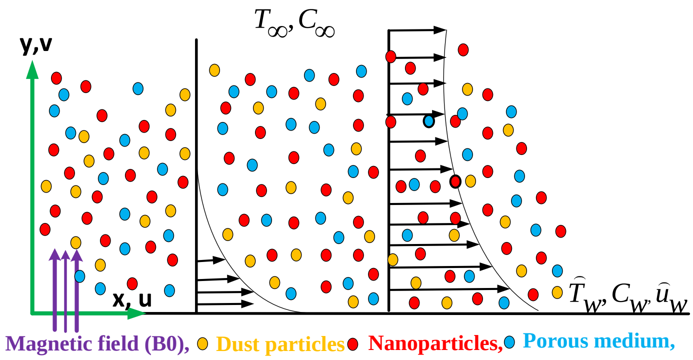

Figure 1. Flow diagram.

$$\frac{\partial \hat{u}}{\partial x}+\frac{\partial \hat{v}}{\partial y}=0, \tag{1}$$

$$\hat{u}\frac{\partial \hat{u}}{\partial x}+\hat{v}\frac{\partial \hat{u}}{\partial y}=\nu\left(1+\frac{1}{\Gamma}\right)\frac{\partial^2 \hat{u}}{\partial y^2}-\frac{\sigma B_0^2}{\rho}\hat{u}-\frac{\nu}{k^*}\hat{u}-F\hat{u^2}+\frac{KN}{\rho}(\hat{u_p}-\hat{u}), \tag{2}$$

$$\begin{aligned}&\left(\hat{u}\frac{\partial T}{\partial x}+\hat{v}\frac{\partial T}{\partial y}+\lambda_1\left[\hat{u}\frac{\partial \hat{u}}{\partial x}.\frac{\partial \hat{T}}{\partial x}+\hat{v}\frac{\partial \hat{v}}{\partial y}.\frac{\partial \hat{T}}{\partial y}+\hat{u}\frac{\partial \hat{v}}{\partial x}.\frac{\partial \hat{T}}{\partial y}+\hat{v}\frac{\partial \hat{u}}{\partial y}.\frac{\partial \hat{T}}{\partial x}+2\hat{u}\hat{v}\frac{\partial^2 T}{\partial x\partial y}+\hat{u}^2\frac{\partial^2 T}{\partial x^2}+\hat{v}^2\frac{\partial^2 T}{\partial y^2}\right]\right)\\ &=k\frac{\partial^2 T}{\partial y^2}+\tau\left[D_B\frac{\partial C}{\partial y}.\frac{\partial T}{\partial y}+\frac{D_T}{T_\infty}\left(\frac{\partial T}{\partial y}\right)^2\right]+\frac{\rho_p C_p}{\rho_{cp}\tau_T}(T_p-T),\end{aligned} \tag{3}$$

$$\hat{u}\frac{\partial C}{\partial x}+\hat{v}\frac{\partial C}{\partial y}=D_B\frac{\partial^2 C}{\partial y^2}+\frac{D_T}{T_\infty}\frac{\partial^2 T}{\partial y^2}+\frac{\rho_p}{\rho\tau_C}(C_p-C). \tag{4}$$

For dusty particle flow

$$\frac{\partial \hat{u_p}}{\partial x}+\frac{\partial \hat{v_p}}{\partial y}=0, \tag{5}$$

$$\hat{u_p}\frac{\partial \hat{u_p}}{\partial x}+\hat{v_p}\frac{\partial \hat{u_p}}{\partial y}=\frac{KN}{\rho}(\hat{u}-\hat{u_p}), \tag{6}$$

$$\hat{u}\frac{\partial T_p}{\partial x}+\hat{v}\frac{\partial T_p}{\partial y}=\frac{c_p}{c_m\tau_T}(T-T_p), \tag{7}$$

$$\hat{u}\frac{\partial C_p}{\partial x}+\hat{v}\frac{\partial C_p}{\partial y}=\frac{mN}{\rho\tau_c}(C-C_p). \tag{8}$$

where ν is kinematic viscosity, ρ demonstrates the fluid density, k^* is the porous medium permeability, $F=\frac{C_b}{\sqrt{k^*}}$ is the coefficient of inertia of porous material, and $-\frac{\nu}{k^*}\hat{u}-F\hat{u^2}$ is due to non-Darcian porous medium, $K=6\pi\mu r$ is the stoke's drag constant, N is the number density of the dust particle, λ_1 is relaxation time for heat flux, k is thermal conductivity, D_T is thermophoresis diffusion, D_B is Brownian diffusion, τ_T is thermal equilibrium time, c_p is fluid specific heat capacity, c_m is dust particle specific heat, and m is dust particle mass.

The dimensional initial and boundary constraints are as follows:

$$\left.\begin{aligned}&\hat{u}=u_w=cx,\hat{v}=0,\ T=T_w,\ C=C_w,\ at\ y=0,\\ &\hat{u_p}=u_w=ax,\hat{v_p}=v,\ T_p=T_w,\ C_p=C_w,\ at\ y=0,\\ &\hat{u}\to 0,\hat{v}\to 0,\ \hat{T}\to T_\infty,\ \hat{C}\to C_\infty,\ at\ y\to\infty,\\ &\hat{u_p}\to 0,\hat{v_p}\to 0,\ \hat{T_p}\to T_\infty,\ \hat{C_p}\to C_\infty,\ at\ y\to\infty.\end{aligned}\right\} \tag{9}$$

The following transformations are introduced for converting the leading differential Equations [40]:

$$\left.\begin{aligned} \hat{u} = cxF'(\eta),\ \hat{v} = -\sqrt{c\nu}F(\eta),\ \eta = \left(\frac{a}{\nu}\right)^{\frac{1}{2}} y, \\ \theta(\eta) = \frac{T - T_\infty}{T_w - T_\infty},\ \phi = \frac{C - C_\infty}{C_w - C_\infty}, \\ \hat{u_p} = axF_p'(\eta),\ \hat{v_p} = -\sqrt{a\nu}F_p(\eta),\ \eta = \sqrt{\frac{a}{\nu}}y, \\ \theta_p(\eta) = \frac{T_p - T_\infty}{T_w - T_\infty},\ \phi_p = \frac{C_p - C_\infty}{C_w - C_\infty}, \end{aligned}\right\} \tag{10}$$

where η represents the similarity variable. $\hat{u}$ (x-axis), and $\hat{v}$ (y-axis) are the velocity components. The temperature of fluid is represented by T and C stands for fluid concentration. T_w, and C_w is the temperature and concentration at the surface. T_∞, is ambient temperature, and C_∞ is fluid ambient concentration. Similarly u_p, v_p are components of velocity of dust particles. T_p and C_p are the temperature, and concentration of dust particles.

After employing similarity transformation, the continuity Equations (1) and (5) are satisfied. However, Equations (2)–(4) and (6)–(8) are transmuted into the dimensionless form:

$$\left(1 + \frac{1}{\Gamma}\right)F''' + FF'' - (M + K_p)F' - (1 + Fr)F'^2 + \Gamma_v.\beta_v(F_p' - F') = 0, \tag{11}$$

$$\frac{1}{Pr}\theta'' + F\theta' - \lambda_t(FF'\theta' + F^2\theta'') + Nb\theta'\phi' + Nt\theta'^2 + \gamma_t.\beta_t(\theta_p - \theta), \tag{12}$$

$$\phi'' + ScF\phi' + \frac{Nt}{Nb}\theta'' + \gamma_c.\beta_c(\phi_p - \phi) = 0. \tag{13}$$

For dusty phase

$$F_pF_p'' - F_p'^2 + \beta_v(F_p' - F') = 0, \tag{14}$$

$$F_p\theta_p' + \gamma_t.\beta_t(\theta - \theta_p) = 0, \tag{15}$$

$$F_p\phi_p' + \gamma_c.\beta_c(\phi - \phi_p) = 0, \tag{16}$$

with the following dimensionless physical constraints:

$$\left.\begin{aligned} &F(\eta) = 0,\ F'(\eta) = 1, \theta(\eta) = 1,\ \phi(\eta) = 1,\ at\ \eta = 0, \\ &F_p(\eta) = F(\eta),\ F_p'(\eta) = 0, \theta_p(\eta) = 1,\ \phi_p(\eta) = 1,\ at\ \eta = 0, \\ &F'(\eta) \to 0,\ \theta(\eta) \to 0,\ \phi(\eta) \to 0,\ at\ \eta \to \infty. \\ &F_p(\eta) \to 0,\ \theta_p(\eta) \to 0,\ \phi_p(\eta) \to 0,\ at\ \eta \to \infty. \end{aligned}\right\} \tag{17}$$

where Γ is the Casson Parameter, $M = \frac{\sigma B_0^2}{\rho c}$ is the magnetic parameter, $Fr = \frac{C_b}{\sqrt{k^*}}$ is the inertia coefficient, $\Gamma_v = \frac{Nm}{\rho}$ is the mass concentration of dusty granules, $\beta_v = \frac{1}{\tau_v c}$ is the interaction parameter for the velocity of a fluid particle, $\tau_v = \frac{m}{K}$ is the dust particle relaxation time, $\rho_p = mN$ is the dust particle density, $\gamma_c = \frac{c_p}{c_m}$ is the specific heat ratio, $Nb = \frac{\tau D_B(C_w - C_\infty)}{\nu}$ is Brownian motion, $Pr = \frac{\mu c_p}{k}$ is the Prandtl number, $\lambda_t = \lambda_1 c$ is the relaxation time parameter, $Nt = \frac{\tau D_T(T_w - T_\infty)}{\nu T_\infty}$ is the thermophoretic parameter, $\beta_t = \frac{1}{c\tau_T}$ is fluid interaction temperature parameter and $Sc = \frac{\nu}{D_B}$ is the Schmidt number.

3. Physical Quantities

The influence of the significant engineering parameters may be adequately investigated in this physical problem by calculating the localized magnitude of drag forces and the rate of thermal transport at the slender sheet. In terms of C_{fx}(skin friction) , Nu_x (Nusselt number) and Sh_x (Sherwood number) are as follows:

$$C_{fx} = \frac{-\tau_w}{\rho u_w^2}, \tag{18}$$

$$Nu_x = \frac{xq_T}{k(T_w - T_\infty)}, \tag{19}$$

$$Sh_x = \frac{xq_w}{D_B(\hat{C} - C_\infty)}, \tag{20}$$

where q_T, and q_w are the heat flux, and mass flux, respectively,

$$\tau_w = \mu(1 + \Gamma^{-1})\left(\frac{\partial \hat{u}}{\partial y}\right)_{y=0} \tag{21}$$

$$q_T = -k\left(\frac{\partial T}{\partial y}\right)_{y=0}, \tag{22}$$

$$q_w = -D_B\left(\frac{\partial C}{\partial y}\right)_{y=0}. \tag{23}$$

implementing the above equations, the following terms are obtained,

$$Re_x^{\frac{1}{2}} C_{fx} = -(1 + \Gamma^{-1})f''(0), \tag{24}$$

$$Re_x^{\frac{-1}{2}} Nu_x = (-\theta'(0)), \tag{25}$$

$$Re_x^{\frac{-1}{2}} Sh_x = (-\phi'(0)). \tag{26}$$

The local Reynolds number $Re_x = \frac{u_w^2}{c\nu}$.

4. Solution Procedure

A system of ordinary differential Eqs represents the flow model. Equations (11)–(16) subjected to boundary conditions (17) are solved using the Runge–Kutta approach along shooting technique using MATLAB software because this scheme is stable, easy to implement and self-starting. The numerical results of flow and heat transfer for the two-phase flow of dusty Casson fluid are determined in terms of velocity and temperature profiles with the influences of several physical parameters. The Runge–Kutta technique has been used to transform the system of ODEs (11)–(16) into first-order ODEs for a solution as follows [42,43]:

$$\begin{aligned}
&f_1' = f_2,\\
&f_2' = f_3,\\
&f_3' = \tfrac{(-1)}{(1+\Gamma^{-1})}[f_1 f_3 - (M + K_p)f_2 - (1 + Fr)f_2^2 + \Gamma_v \beta_v (f_9 - f_2)],\\
&f_4' = f_5,\\
&f_5' = \tfrac{(-1)}{(\frac{1}{Pr}+\lambda f_1^2)}[f_1 f_5 + \Lambda_t f_1 f_2 f_5 + Nb f_5 f_7 + Nt f_5^2 + \gamma_t \beta_t (f_{10} - f_4)],\\
&f_6' = f_7,\\
&f_7' = (-1)[Sc f_1 f_7 + \tfrac{Nt}{Nb} f_5' + \gamma_c \beta_c (f_{12} - f_6)],\\
&f_8' = f_9\\
&f_9' = \tfrac{(-1)}{f_8}[\beta_v (f_9 - f_2) - f_9^2],\\
&f_{10}' = \tfrac{(-1)}{f_8}[\gamma_t \beta_t (f_4 - f_{10})],
\end{aligned}$$

$$f_{11}' = \frac{(-1)}{f_8}[\gamma_c\beta_c(f_6 - f_{11})],$$

and the boundary conditions (17) are enumerated as

$$\begin{aligned}
&f_1 = 0,\ f_2 = 1,\ f_4 = 0,\ f_6 = 1f_3,\ at\ \eta = 0,\\
&f_8 = f_1,\ f_9 = 0,\ f_{10} = 1,\ f_{11} = 1,\ at\ \eta = 0,\\
&f_2 \to 0,\ f_5 \to 0,\ f_6 \to 0,\ as\ \eta \to \infty.\\
&f_8 \to 0,\ f_{10} \to 0,\ f_{11} \to 0,\ as\ \eta \to \infty.
\end{aligned}$$

5. Results and Discussion

This research aims to begin to investigate Casson fluid boundary layer flow and melting thermal transport across a stretched surface with fluid-particle suspension, melting effect, and Cattaneo–Christov heat flux. The Runge–Kutta approach is used to solve the governed highly nonlinear expressions with associated conditions and is coded in MATLAB. The numerical code validation is obtained by comparing the numerical outcomes of the current and past results of skin friction (Gireesha [44], Jalil [40]). Our findings are obtained to be in good agreement with them (see Table 1). The impact of parameters on momentum, thermal, and concentration layers in dual fluid and dusty phases. We take values of parameters as $\Gamma = 0.5, M = 0.5, Sc = 2.0, Pr = 2.0, K_p = 0.3, Nb = Nt = 0.2, \lambda_t = 0.1, \gamma_v = \beta_v = 1.0, \gamma_t = \beta_t = 0.2, \gamma_c = \beta_c = 1.0$.

The effect of magnetic parameter M on momentum boundary layer $F'(\eta)$, dust phase velocity $F_p(\eta)$ is portrayed in Figure 2a,b, it is noticed that improving the values of M lowers the velocity profiles in both fluid $F'(\eta)$, and dusty phase $F_p(\eta)$. The enhanced M causes a greater opposing (Lorentz force) force on the stream, slowing it down. On the other hand, the Casson parameter Γ also diminishes for fluid and dust phase velocity. Improvement in Γ leads to enhanced dynamic viscosity, induces deficiency in fluid flow, and diminishes velocity for fluid and dust. The drawing for fluid temperature $\theta(\eta)$, fluid concentration $\phi(\eta)$ and dust phase temperature $\theta_p(\eta)$ and dust concentration $\phi_p(\eta)$ as influenced by M are portraited in Figures 3a,b and 4a,b. Increasing the value of M rises the curve for fluid and dust phase temperature and concentration profile. The increase in M causes the stronger the resistive force. Meanwhile, the fluid loss of kinetic energy is offset by a gain in heat energy, and then the temperature and concentration are enhanced. Casson parameter Γ also enhanced fluid temperature, concentration, and dust phase. Improvement in Γ enhanced temperature and fluid and dust concentration.

Figure 5a,b are portraits of the impacts of K_p for both fluid and dusty particles. From these, it is observed that by increasing the values of K_p depreciation in velocity and momentum boundary layer thickness, caused due to K_p ($K_p = \frac{\nu}{K^*a}$) is converse to the permeability k^* of the porous medium. The higher inputs K_p means lower k^* and hence higher resistance is offered to the flow to the velocity and rise in temperature and concentration for both fluid and dusty phase portraits in Figures 6a,b and 7a,b. Similarly, local inertia parameter Fr on velocity for fluid and dust diminished for growing values of Fr, caused due to inertia coefficient is a direct relation to medium porosity and drag force. So when Cb enhances, the liquid resistive force is stronger, velocity is lower for the fluid and dust phase and rise in temperature and concentration for fluid and dust particles. The influence of temperature distribution of Casson nanofluid and dust phase θ and θ_p depicted in Figure 8a,b. The larger values of Nb, the faster the nanoparticles migrate, increasing heat diffusion and then rising in temperature for both phases. The quick motion also impairs focus. Thermophoretic impact happens when particles go from hot to cold. The dependence of the relaxation time parameter Γ on the temperature distribution for both Casson fluid and dusty phases is portrayed in Figure 9a,b. As can be seen in this diagram, as the relaxation time parameter increases, the temperature distribution (θ, θ_p) and thickness of the thermal boundary layer decline. Physically, it indicates that the relaxation time parameter's progressive nature necessitates a longer time for thermal transport from densely packed fluid particles to lowenergy fluid particles. As a result, both the fluid and dust phases decrease the temperature distribution.

Figure 9a,b are also depicted to understand the effect of specific heat ratio parameter γ_t on the temperature profile. It is noticed that the thermal boundary layer thickness and temperature profile for both fluid and dust phases diminished by enhancing specific heat ratio. Brownian motion Nb affects fluid concentration distribution and dust phase elucidated in Figure 10a,b. By growing Nb, the fluid concentration and dust phase are lower. The thermal energy is contributed by nanoparticle dispersion and random motion, and festally distributed particles have a lower fluid concentration and dust phases. The thermophoresis effect represents the movement of nanoparticles from an upper to a lower temperature. As a result, as shown in Figure 10a,b, concentration ϕ, ϕ_p rises in an indirect relationship with Nt. The variations in Nusselt Nu_x and Sherwood Sh_x are shown in Figure 11a,b. The parameters Nt, Nb, and M offer various values. With modest increases in similar values of Nb and Nt, the amount Nusselt decreases noticeably, although Sheroowd achieves larger values in this scenario. The effect of skin friction C_{fx} and Nusselt number Nu_x are visible in Figure 12a,b. The parameters M, K_p and Γ give different values. Increase in values of K_P sand Γ the skin friction and Nusselt number decrease.

Table 1. The skin friction coefficient was compared for different inputs of β_t and M while all other parameters were ignored.

M	Gireesha et al. [44] $\beta_v = 0$	Jalil et al. [40] $\beta_v = 0$	Our Results $\beta_v = 0$	Gireesha et al. [44] $\beta_v = 0.5$	Jalil et al. [40] $\beta_v = 0.5$	Our Results $\beta_v = 0.5$
0.2	1.0000	1.000000	1.0000	1.034	1.033505	1.0335
0.2	1.095	1.095445	1.0955	1.126	1.126114	1.1261
0.5	1.224	1.224745	1.2248	1.252	1.252251	1.2523
1.0	1.414	1.414214	1.4142	1.438	1.438101	1.4381
1.2	1.483	1.483240	1.4832	1.506	1.506032	1.5060
1.5	1.581	1.581139	1.5901	1.602	1.602540	1.6026
2.0	1.732	1.732051	1.8301	1.751	1.751609	1.7517

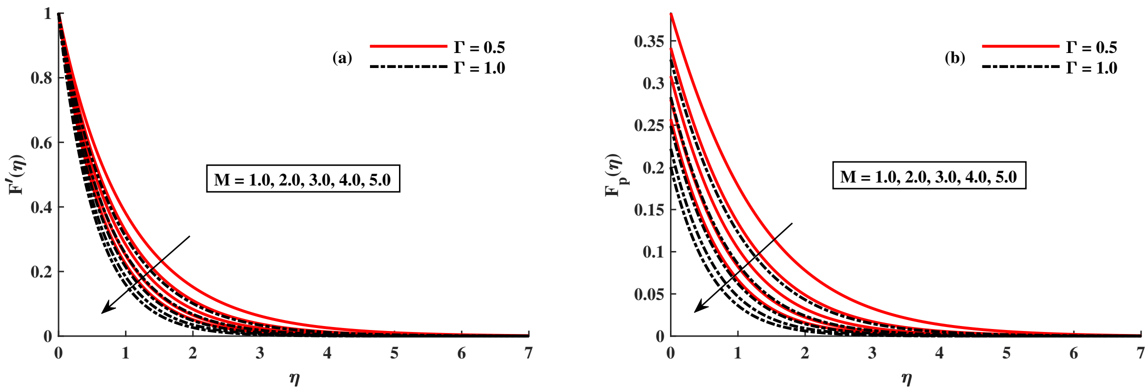

Figure 2. Variation of M to influence the fluid and dust velocity profile.

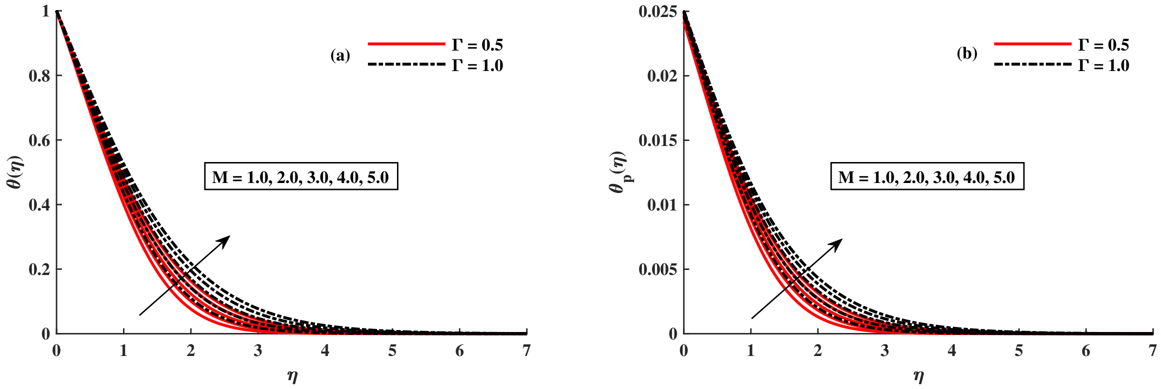

Figure 3. Variation of M to influence the fluid and dust temperature profile.

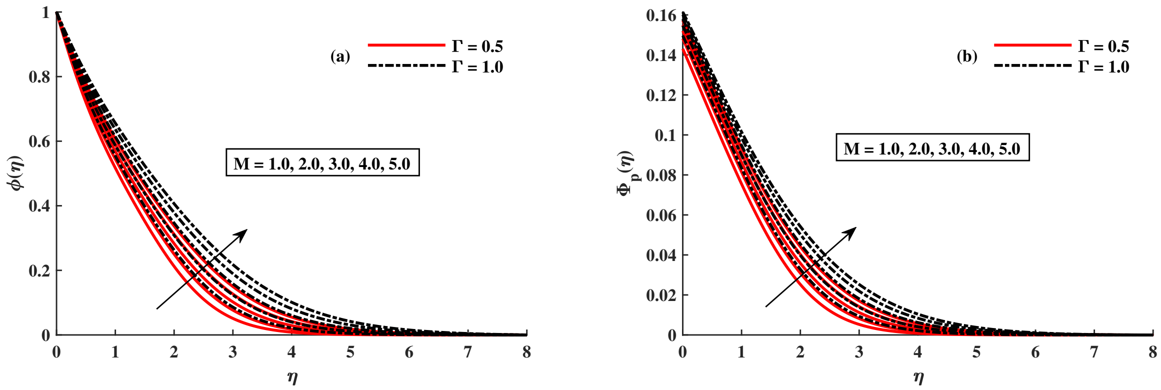

Figure 4. Variation of M to influence the fluid and dust concentration profile.

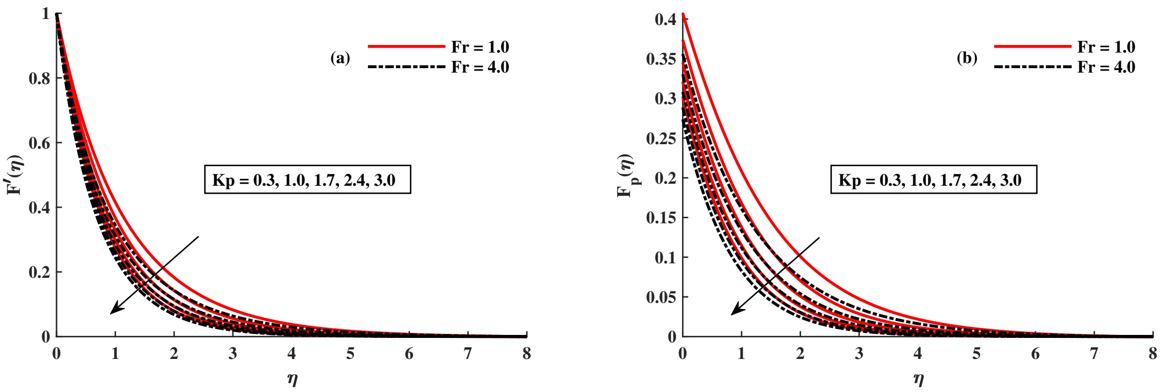

Figure 5. Variation of K_p to influence the fluid and dust velocity profile.

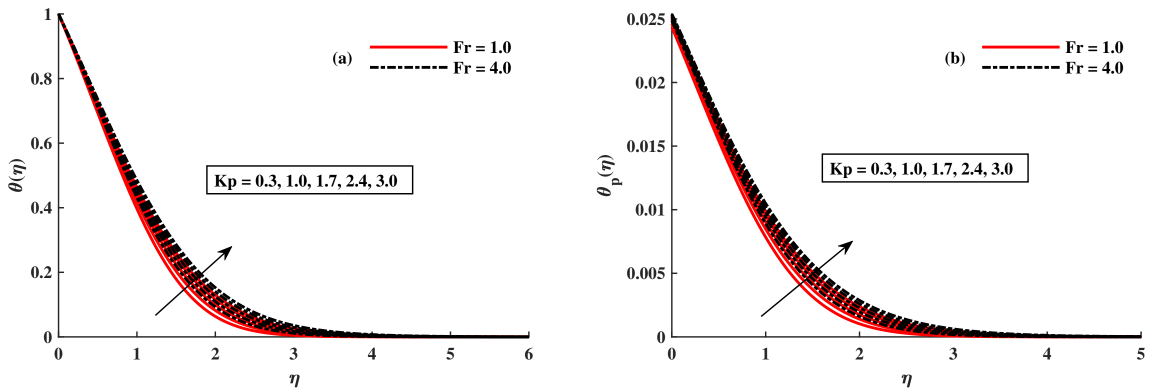

Figure 6. Variation of K_p to influence the fluid and dust temperature profile.

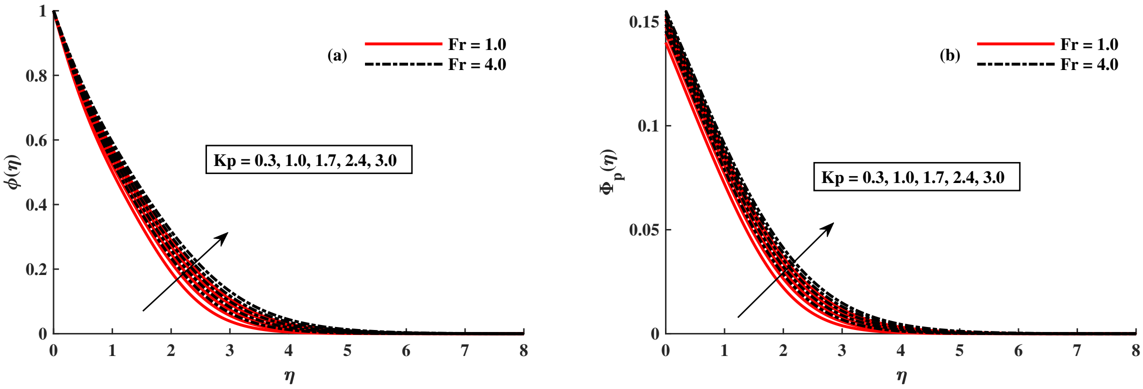

Figure 7. Variation of K_p to influence the fluid and dust concentration profile.

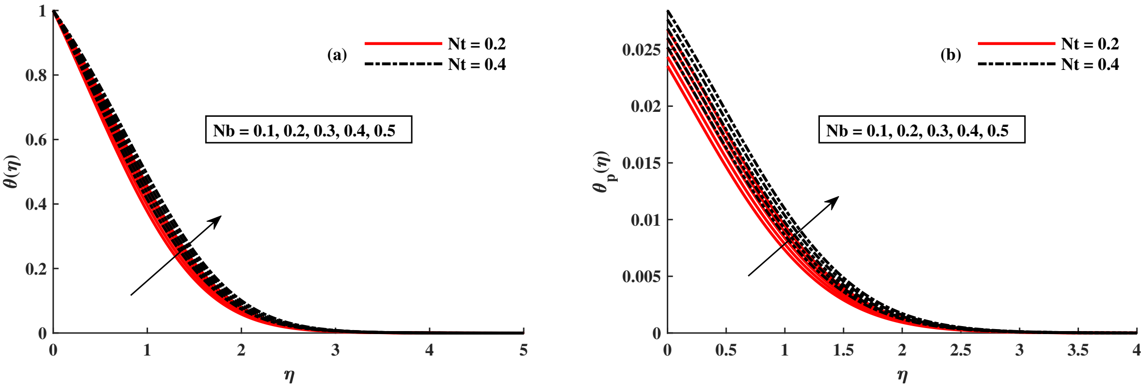

Figure 8. Variation of Nb to influence the fluid and dust temperature profile.

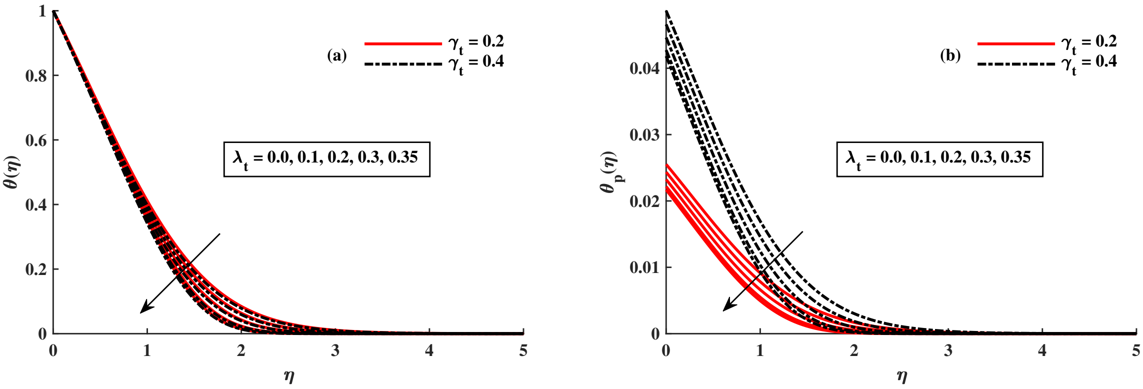

Figure 9. Variation of λ_t to influence the fluid and dust temperature profile.

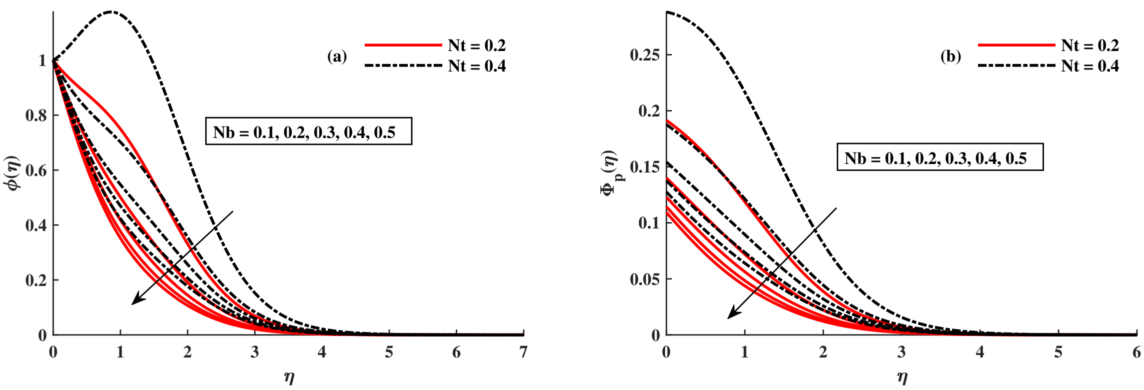

Figure 10. Variation of Nb to influence the fluid and dust concentration profile.

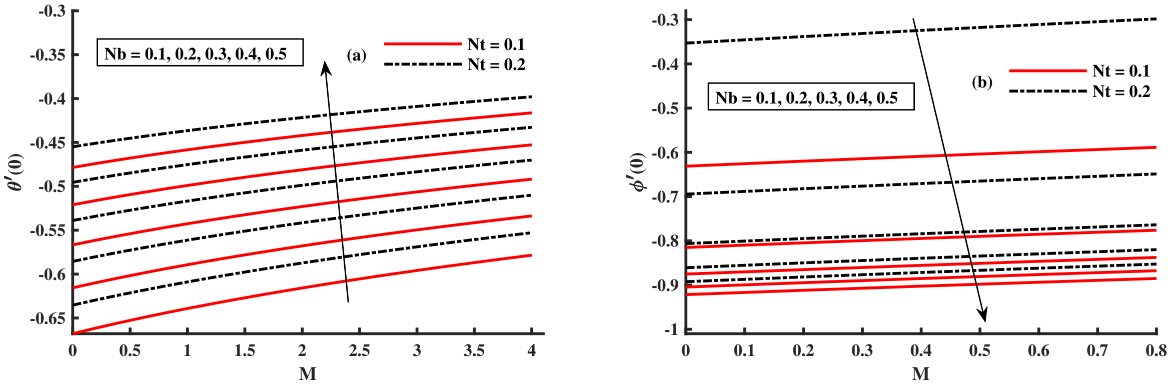

Figure 11. Variation of Nusselt number Nu_x and Sheroowd number Sh_x along M, Nb and Nt.

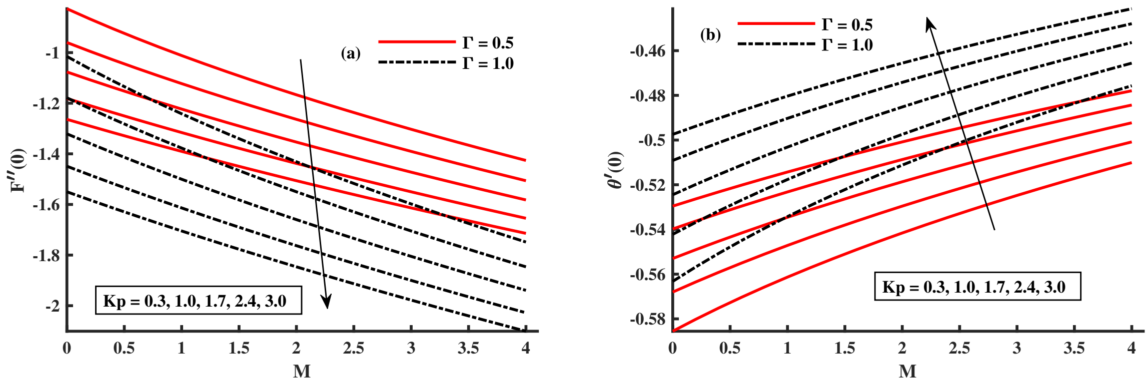

Figure 12. Variation of skin friction C_{fx} and Nusselt number Nu_x along M, K_p and Γ.

6. Conclusions

In the majority of the industrial, science and engineering processes convection is nonlinear. It offers a wide range of uses, including large surface area, electron mobility, and stability. It possesses exceptional electrical, optical, material, physical, and chemical characteristics. In this research, we have examined the role of modified Fourier law in the flow of an MHD Casson nanofluid flow with dust particles over a stretched surface. The combined effect of Brownian motion and thermophoresis in nanofluid modeling is retained. Firstly, the partial differential expressions are transmuted into ordinary differential equations by implementing a similarity approach. Afterward, the solutions of attained equations are solved by implementing the Runge–Kutta–Fehlberg–45 method. A comparison is also made with a published paper to ascertain the validity of the presented model. The key observations of this study are listed below:

- The impacts of porosity, Forchheimer and magnetic parameters on fluid flow show decreasing behavior for both fluid and dust phases.
- The temperature profile increases as porosity, Forchheimer and magnetic parameters are augmented, but the reverse behavior is viewed when the values of λ_t increase for both dust and fluid phase.
- Brownian diffusion enhanced the temperature profile and reduced the concentration profile.
- The current results were compared with the available results in the existing literature for the special case, and there was good agreement between them showing the validation of the present study.
- The growing strength of magnetic field (M), porosity (K_p), and Casson fluid parameter (Γ) caused to decline in the skin friction and Nusselt number.

This analysis may be extended for the hybrid-based dusty nano liquid, Williamson dusty fluid, Oldroyd-B dusty fluid and other non-Newtonian dusty fluids.

Author Contributions: Data curation, N.A.S.; Formal analysis, J.D.C.; Investigation, L.A.; Methodology, N.F.; Software, B.A.; Validation, M.I. and J.D.C.; Writing—original draft, S.U.R.; Writing—review & editing, N.A.S. All authors have read and agreed to the published version of the manuscript.

Funding: This research received no external funding.

Institutional Review Board Statement: Not Applicable.

Informed Consent Statement: Not Applicable.

Data Availability Statement: Not Applicable.

Conflicts of Interest: The authors declare no conflict of interest.

Acknowledgments: This work was supported by the Technology Innovation Program (20018869, Development of Waste Heat and Waste Cold Recovery Bus Air-conditioning System to Reduce Heating and Cooling Load by 10%) funded By the Ministry of Trade, Industry & Energy(MOTIE, Korea).

Nomenclature

$\hat{u}$	Fluid velocity components along the x-axis	$\hat{v}$	Fluid velocity components along the y-axis
ρ_f	Density of fluid	ρ_p	Density of dust particles
ν	Kinematic viscosity of fluid	Γ	Casson parameter
σ	Electrical conductivity	B_0	Magnetic field strength
k^*	Permeability of porous medium	F	Co-efficient of inertia of porous material
K	Stoke's drag constant	N	Dust particle number constant
m	Mass of dust particle	τ_T	Thermal equilibrium time
λ_1	Relaxation time for heat flux	c_m	Specific heat of dust particle
T	non-dimensional temperature	T_w	Temperature at surface
C	non-dimensional nanoparticles concentration	C_w	Concentration at surface
C_p	Concentration of dust particles	μ	Dynamic viscosity
T_∞	temperature away from the surface, K	c_p	Specific heat capacity of the fluid
C_∞	concentration away from the surface	Ω	angular velocity
T_p	Temperature of the dust particle	u_w	velocity of stretching sheet
Cf_x	skin friction at x-direction	$(\hat{u}_p, \hat{v}_p)$	Velocity components of dust particles
Nu_x	Nusselt number	Sh_x	Sherwood number
k	Thermal conductivity	Nb	Brownian motion parameter
Nt	thermophoresis parameter	Cp	Specific heat and constant pressure

References

1. Saffman, P. On the stability of laminar flow of a dusty gas. *J. Fluid Mech.* **1962**, *13*, 120–128. [CrossRef]
2. Chakrabarti, K. Note on boundary layer in a dusty gas. *AIAA J.* **1974**, *12*, 1136–1137. [CrossRef]
3. Datta, N.; Mishra, S. Boundary layer flow of a dusty fluid over a semi-infinite flat plate. *Acta Mech.* **1982**, *42*, 71–83. [CrossRef]
4. Wei, Y.; Rehman, S.U.; Fatima, N.; Ali, B.; Ali, L.; Chung, J.D.; Shah, N.A. Significance of dust particles, nanoparticles radius, coriolis and lorentz forces: The case of maxwell dusty fluid. *Nanomaterials* **2022**, *12*, 1512. [CrossRef] [PubMed]
5. Anwar, M.I.; Firdous, H.; Zubaidi, A.A.; Abbas, N.; Nadeem, S. Computational analysis of induced magnetohydrodynamic non-Newtonian nanofluid flow over nonlinear stretching sheet. *Prog. React. Kinet. Mech.* **2022**, *47*, 14686783211072712. [CrossRef]
6. Kumar, D.; Sahu, A.K. Non-newtonian fluid flow over a rotating elliptic cylinder in laminar flow regime. *Eur. J. Mech.-B/Fluids* **2022**, *93*, 117–136. [CrossRef]
7. Khashi'ie, N.S.; Waini, I.; Kasim, A.R.M.; Zainal, N.A.; Ishak, A.; Pop, I. Magnetohydrodynamic and viscous dissipation effects on radiative heat transfer of non-newtonian fluid flow past a nonlinearly shrinking sheet: Reiner–philippoff model. *Alex. Eng. J.* **2022**, *61*, 7605–7617. [CrossRef]
8. Chaudhuri, S.; Chakraborty, P.; Das, M.; Das, B. Magnetohydrodynamic mixed convection in a non-Newtonian third-grade fluid flowing through vertical parallel plates: A semianalytical study of flow and heat transfer. *Heat Transfer* **2022**, *51*, 3373–3400. [CrossRef]
9. Khan, S.U.; Al-Khaled, K.; Hussain, S.M.; Ghaffari, A.; Khan, M.I.; Ahmed, M.W. Implication of arrhenius activation energy and temperature-dependent viscosity on non-newtonian nanomaterial bio-convective flow with partial slip. *Arab. J. Sci. Eng.* **2022**, *47*, 7559–7570. [CrossRef]

10. Riaz, A.; Awan, A.U.; Hussain, S.; Khan, S.U.; Abro, K.A. Effects of solid particles on fluid-particulate phase flow of non-newtonian fluid through eccentric annuli having thin peristaltic walls. *J. Therm. Anal. Calorim.* **2022**, *147*, 1645–1656. [CrossRef]
11. Khan, M.I.; Alzahrani, F. Numerical simulation for the mixed convective flow of non-newtonian fluid with activation energy and entropy generation. *Math. Methods Appl. Sci.* **2021**, *44*, 7766–7777. [CrossRef]
12. Reddy, M.G.; Rani, M.S.; Praveen, M.; Kumar, K.G. Comparative study of different non-newtonian fluid over an elaborated sheet in the view of dual stratified flow and ohmic heat. *Chem. Phys. Lett.* **2021**, *784*, 139096. [CrossRef]
13. Fatunmbi, E.O.; Okoya, S.S. Quadratic mixed convection stagnation-point flow in hydromagnetic casson nanofluid over a nonlinear stretching sheet with variable thermal conductivity. In *Defect and Diffusion Forum*; Trans Tech Publ: Stafa-Zurich, Switzerland, 2021; Volume 409, pp. 95–109.
14. Fatunmbi, E.; Okoya, S. Electromagnetohydrodynamic micropolar-casson fluid boundary layer flow and heat transfer over a stretching material featuring temperature-based thermophysical properties in a porous medium. *J. Niger. Math. Soc.* **2021**, *40*, 245–268.
15. Sandhya, A.; Reddy, G.R.; Deekshitulu, G. Heat and mass transfer effects on MHD flow past an inclined porous plate in the presence of chemical reaction. *Int. J. Appl. Mech. Eng.* **2020**, *25*, 86–102. [CrossRef]
16. Kumar, B.; Srinivas, S. Unsteady hydromagnetic flow of Eyring–Powell nanofluid over an inclined permeable stretching sheet with joule heating and thermal radiation. *J. Appl. Comput. Mech.* **2020**, *6*, 259–270.
17. Hussain, F.; Abdal, S.; Abbas, Z.; Hussain, N.; Adnan, M.; Ali, B.; Zulqarnain, R.M.; Ali, L.; Younas, S. Buoyancy effect on MHD slip flow and heat transfer of a nanofluid flow over a vertical porous plate. *Sci. Inq. Rev.* **2020**, *4*, 1–16. [CrossRef]
18. Rehman, S.U.; Mariam, A.; Ullah, A.; Asjad, M.I.; Bajuri, M.Y.; Pansera, B.A.; Ahmadian, A. Numerical computation of buoyancy and radiation effects on MHD micropolar nanofluid flow over a stretching/shrinking sheet with heat source. *Case Stud. Therm. Eng.* **2021**, *25*, 100867. [CrossRef]
19. Hayat, T.; Riaz, R.; Aziz, A.; Alsaedi, A. Influence of arrhenius activation energy in MHD flow of third grade nanofluid over a nonlinear stretching surface with convective heat and mass conditions. *Phys. A Stat. Mech. Its Appl.* **2020**, *549*, 124006. [CrossRef]
20. Kardri, M.A.; Bachok, N.; Arifin, N.M.; Ali, F.M.; Rahim, Y.F. Magnetohydrodynamic flow past a nonlinear stretching or shrinking cylinder in nanofluid with viscous dissipation and heat generation effect. *J. Adv. Res. Fluid Mech. Therm. Sci.* **2022**, *90*, 102–114. [CrossRef]
21. Fetecau, C.; Shah, N.A.; Vieru, D. General solutions for hydromagnetic free convection flow over an infinite plate with newtonian heating, mass diffusion and chemical reaction. *Commun. Theor. Phys.* **2017**, *68*, 768. [CrossRef]
22. Khan, M.I.; Hafeez, M.; Hayat, T.; Khan, M.I.; Alsaedi, A. Magneto rotating flow of hybrid nanofluid with entropy generation. *Comput. Methods Programs Biomed.* **2020**, *183*, 105093. [CrossRef] [PubMed]
23. Shoaib, M.; Raja, M.A.Z.; Sabir, M.T.; Islam, S.; Shah, Z.; Kumam, P.; Alrabaiah, H. Numerical investigation for rotating flow of MHD hybrid nanofluid with thermal radiation over a stretching sheet. *Sci. Rep.* **2020**, *10*, 1–15. [CrossRef] [PubMed]
24. Hussain, T.; Xu, H.; Raees, A.; Zhao, Q.-K. Unsteady three-dimensional MHD flow and heat transfer in porous medium suspended with both microorganisms and nanoparticles due to rotating disks. *J. Therm. Anal. Calorim.* **2022**, *147*, 1607–1619. [CrossRef]
25. Krishna, M.V.; Ahamad, N.A.; Chamkha, A.J. Numerical investigation on unsteady MHD convective rotating flow past an infinite vertical moving porous surface. *Ain Shams Eng. J.* **2021**, *12*, 2099–2109. [CrossRef]
26. Jiang, Y.; Sun, H.; Bai, Y.; Zhang, Y. Mhd flow, radiation heat and mass transfer of fractional burgers' fluid in porous medium with chemical reaction. *Comput. Math. Appl.* **2022**, *115*, 68–79. [CrossRef]
27. Hossain, R.; Azad, A.; Hasan, M.J.; Rahman, M. Radiation effect on unsteady mhd mixed convection of kerosene oil-based cnt nanofluid using finite element analysis. *Alex. Eng. J.* **2022**, *61*, 8525–8543. [CrossRef]
28. Ghasemi, S.; Hatami, M. Solar radiation effects on mhd stagnation point flow and heat transfer of a nanofluid over a stretching sheet. *Case Stud. Therm. Eng.* **2021**, *25*, 100898. [CrossRef]
29. Mandal, D.K.; Biswas, N.; Manna, N.K.; Gorla, R.S.R.; Chamkha, A.J. Role of surface undulation during mixed bioconvective nanofluid flow in porous media in presence of oxytactic bacteria and magnetic fields. *Int. J. Mech. Sci.* **2021**, *211*, 106778. [CrossRef]
30. Choi, S.U.; Eastman, J.A. *Enhancing Thermal Conductivity of Fluids with Nanoparticles*; Tech. Rep.; Argonne National Lab.: Lemont, IL, USA, 1995.
31. Khan, M.; Malik, M.; Salahuddin, T.; Hussian, A. Heat and mass transfer of Williamson nanofluid flow yield by an inclined lorentz force over a nonlinear stretching sheet. *Results Phys.* **2018**, *8*, 862–868. [CrossRef]
32. Saeed, A.; Kumam, P.; Nasir, S.; Gul, T.; Kumam, W. Non-linear convective flow of the thin film nanofluid over an inclined stretching surface. *Sci. Rep.* **2021**, *11*, 18410 . [CrossRef]
33. Yahya, A.U.; Salamat, N.; Huang, W.-H.; Siddique, I.; Abdal, S.; Hussain, S. Thermal charactristics for the flow of Williamson hybrid nanofluid (mos2+ zno) based with engine oil over a streched sheet. *Case Stud. Therm. Eng.* **2021**, *26*, 101196. [CrossRef]
34. Gopal, D.; Saleem, S.; Jagadha, S.; Ahmad, F.; Almatroud, A.O.; Kishan, N. Numerical analysis of higher order chemical reaction on electrically mhd nanofluid under influence of viscous dissipation. *Alex. Eng. J.* **2021**, *60*, 1861–1871. [CrossRef]
35. Gouran, S.; Mohsenian, S.; Ghasemi, S. Theoretical analysis on mhd nanofluid flow between two concentric cylinders using efficient computational techniques. *Alex. Eng. J.* **2022**, *61*, 3237–3248. [CrossRef]

36. Rashidi, M.M.; Nazari, M.A.; Mahariq, I.; Assad, M.E.H.; Ali, M.E.; Almuzaiqer, R.; Nuhait, A.; Murshid, N. Thermophysical properties of hybrid nanofluids and the proposed models: An updated comprehensive study. *Nanomaterials* **2021**, *11*, 3084. [CrossRef]
37. Aly, A.M.; Mohamed, E.M.; Alsedais, N. The magnetic field on a nanofluid flow within a finned cavity containing solid particles. *Case Stud. Therm. Eng.* **2021**, *25*, 100945. [CrossRef]
38. Wang, F.; Rehman, S.; Bouslimi, J.; Khaliq, H.; Qureshi, M.I.; Kamran, M.; Alharbi, A.N.; Ahmad, H.; Farooq, A. Comparative study of heat and mass transfer of generalized mhd oldroyd-b bio-nano fluid in a permeable medium with ramped conditions. *Sci. Rep.* **2021**, *11*, 1–32. [CrossRef]
39. Sheikholeslami, M.; Farshad, S.A.; Ebrahimpour, Z.; Said, Z. Recent progress on flat plate solar collectors and photovoltaic systems in the presence of nanofluid: A review. *J. Clean. Prod.* **2021**, *293*, 126119. [CrossRef]
40. Jalil, M.; Asghar, S.; Yasmeen, S. An exact solution of MHD boundary layer flow of dusty fluid over a stretching surface. *Math. Probl. Eng.* **2017**, *2017*, 2307469. [CrossRef]
41. Haider, S.M.A.; Ali, B.; Wang, Q.; Zhao, C. Stefan blowing impacts on unsteady mhd flow of nanofluid over a stretching sheet with electric field, thermal radiation and activation energy. *Coatings* **2021**, *11*, 1048. [CrossRef]
42. Lou, Q.; Ali, B.; Rehman, S.U.; Habib, D.; Abdal, S.; Shah, N.A.; Chung, J.D. Micropolar dusty fluid: Coriolis force effects on dynamics of mhd rotating fluid when lorentz force is significant. *Mathematics* **2022**, *10*, 2630. [CrossRef]
43. Ashraf, M.Z.; Rehman, S.U.; Farid, S.; Hussein, A.K.; Ali, B.; Shah, N.A.; Weera, W. Insight into significance of bioconvection on mhd tangent hyperbolic nanofluid flow of irregular thickness across a slender elastic surface. *Mathematics* **2022**, *10*, 2592. [CrossRef]
44. Gireesha, B.; Ramesh, G.; Bagewadi, C. Heat transfer in MHD flow of a dusty fluid over a stretching sheet with viscous dissipation. *Adv. Appl. Sci. Res.* **2012**, *3*, 2392–2401.